



Full paper

Insights into the storage mechanism of VS₄ nanowire clusters in aluminum-ion battery

Lingli Xing^a, Kwadwo Asare Owusu^a, Xinyu Liu^a, Jiashen Meng^a, Kun Wang^{b,**}, Qinyou An^a, Liqiang Mai^{a,c,*}

^a State Key Laboratory of Advanced Technology for Materials Synthesis and Processing, Wuhan University of Technology, Wuhan, 430070, PR China

^b State Key Laboratory of Silicate Materials for Architectures, Wuhan University of Technology, Wuhan, 430070, PR China

^c Foshan Xianhu Laboratory of the Advanced Energy Science and Technology Guangdong Laboratory, Xianhu Hydrogen Valley, Foshan, 528200, PR China



ARTICLE INFO

Keywords:

Aluminum-ion batteries
Channels-rich VS₄
Ex-situ X-ray diffraction
In-situ Raman

ABSTRACT

As promising electrode materials for aluminum-ion batteries (AIBs), transition metal sulfides have attracted significant attention. However, the relative low energy density and poor rate property restrict their further applications. Herein, channels-rich VS₄ nanowire clusters were synthesized via an amine ions-assisted method. When assessed as a cathode for rechargeable AIB, the VS₄ nanowire clusters exhibit superior electrochemical performances, specifically, outstanding rate property (103.32 mAh g⁻¹ at 800 mA g⁻¹), good cycling stability and a high reversible capacity of 252.51 mAh g⁻¹ (at 100 mA g⁻¹). Moreover, *ex-situ* X-ray diffraction (XRD) and *in-situ* Raman techniques reveal that the as-prepared VS₄ nanowire clusters have stable channels-rich structures, which is favorable for the mass transfer in electrochemical reaction. A mechanism of intercalation is proposed for the electrochemical process. This work takes a step toward the development of high-performance electrode materials for AIBs and provides new insights into the chemistry of AIBs for electrochemical energy storage.

1. Introduction

Increasing global energy crisis and environmental problems arising from fossil fuel usage have greatly heightened the demand for clean energy technologies including high-performance energy generation and storage devices. Currently, the energy storage market is dominated by lithium-ion batteries (LIBs) due to their high energy density (250 Wh kg⁻¹) [1–3]. However, the scarcity of lithium sources and safety issues associated with flammable organic electrolytes are hindering their further development. Under these circumstances, developing multivalent-ion batteries technologies such as Ca [4], Mg [5], and Al [6] are highly promising for the future of energy storage. Among the various multivalent-ion batteries, aluminum ion battery is an energy storage of choice with great potential to replace LIBs [7]. On the one hand, aluminum metal is extremely cheap (~1.4 USD kg⁻¹) owing to the abundant store (3rd element below O and Si) [8]. On the other hand, the trivalent Al³⁺ allows more ions and electrons to be transferred, which will directly lead to a high theoretical capacity and considerable energy

density when coupled with suitable electrode materials. These positives make AIB a promising new generation large-scale energy storage device [9,10].

Despite their attractive advantages in resource and theoretical energy density, the poor capacity reversibility and slow kinetics of electrodes have hindered research interests into rechargeable AIBs for a long time. As a component of AIBs, cathode materials play an important role, and plenty of materials have been explored, including graphitic materials [11,12], transition metal oxides [13,14] and chalcogenides [15, 16]. Compared with other materials, transition metal chalcogenides (TMCs) are recognized as a promising class of materials not only because of the abundant resources but also their multiple valence. Among TMCs, Co₃S₄, MoS₂, CoSe and CoSe₂ have been reported as cathode materials for AIBs [16–19]. TMCs have more electrons involvement in electrochemical reactions, and thus can realize higher capacity [20,21]. However, due to the instability of these materials, they usually suffer from severe structural damage and huge diffusion resistance. Numerous strategies have been employed to address this challenge, for instance

* Corresponding author. State Key Laboratory of Advanced Technology for Materials Synthesis and Processing, Wuhan University of Technology, Wuhan 430070, PR China,

** Corresponding author.

E-mail addresses: kun.wang@whut.edu.cn (K. Wang), mlq518@whut.edu.cn (L. Mai).

<https://doi.org/10.1016/j.nanoen.2020.105384>

Received 28 July 2020; Received in revised form 6 September 2020; Accepted 9 September 2020

Available online 16 September 2020

2211-2855/© 2020 Elsevier Ltd. All rights reserved.

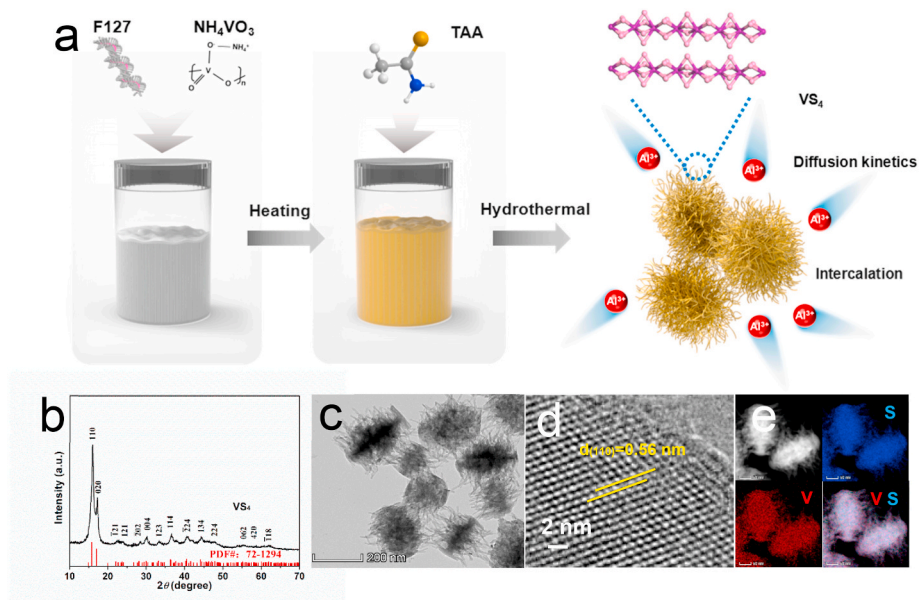


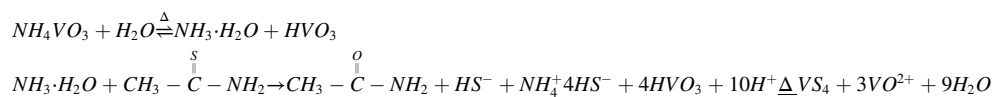
Fig. 1. (a) Formation routine and the “linear-chain” crystalline structure. (b) XRD pattern. (c) TEM image. (d) HRTEM image. (e) HAADF-STEM image and corresponding elemental mapping images of the VS_4 nanowire clusters.

holding cutoff voltage, designing nanomaterials, and synthesizing with graphene [22]. Anyway, enhancing the performance of TMCs to realize high specific capacity and excellent cycle performance is highly challenging. Possessing a unique chain like structure loosely packed by Van Der Waals forces, VS_4 has shown great advantage among various transition metal sulfides. Furthermore, the large interlayer distances endow it with an efficient platform for the fast intercalation/de-intercalation of Al^{3+} ions. Despite such anticipated structural advantages, development of VS_4 for AIBs has remained uncertain to date.

Herein, we report a channels-rich VS_4 nanowire clusters synthesized via an amine-ion assisted method. When tested for rechargeable aluminum-ion battery as cathode, the VS_4 nanowire clusters electrode exhibits exceptional electrochemical performance in comparison with other reported AIBs materials heretofore. The VS_4 nanowire clusters exhibit excellent cycling stability and high reversible capacity of $252.51 \text{ mAh g}^{-1}$ at 100 mA g^{-1} . Moreover, superior rate capability of $103.32 \text{ mAh g}^{-1}$ was achieved at the current density of 800 mA g^{-1} . Structural identifications reveal the as synthesized VS_4 has a nanowire clusters shape which is rich of ion channels, and this shortens the distance of mass transfer and facilitates the fast electrochemical reactions. In addition, *ex-situ* XRD and *in-situ* Raman techniques confirmed that the VS_4 electrode has highly stable ion channels and undergoes almost no obvious pulverization during the Al^{3+} ion intercalation/extraction process. This work proposes a low-cost cathode material for highly reversible AIBs as well as offers new insights into the storage mechanisms of AIBs, which is essential for devising and developing next generation AIBs with outstanding performances.

2. Results and discussion

The straightforward synthesis of the VS_4 nanowire clusters via an amine ion-assisted method is schematically depicted in Fig. 1a. The relevant chemical reactions are proposed as follows:



As shown in Fig. 1b, the XRD pattern showed good crystallinity and high purity of the VS_4 nanowire clusters (JCPDS: 72–1294). All diffraction peaks can be clearly assigned to monoclinic phase VS_4 . SEM images (Figure S1a-b) demonstrate that these products show multi-nanowires morphology, the nanowire cluster with a width of circa 250 nm and a length of circa 260 nm, the nanowire with a width of circa 20 nm and a length of circa 80 nm. In practice, their relatively short diffusion lengths could enhance the electrochemical as well as kinetic properties. Moreover, the TEM image (Fig. 1c) of VS_4 reveals a porous surface structure. The rough surface enhances the tight contact between the electrode and the electrolyte, which is favorable for excellent rate performance [23].

The HRTEM image (Fig. 1d) displays the inter planar spacing of 0.56 nm was in agreement with (110) plane of VS_4 . Selected area electron diffraction (SAED) pattern (Figure S1c) of the VS_4 nanowire clusters further confirms its polycrystalline nature. These diffraction rings correspond to (110), ($\bar{1}$ 202), ($\bar{1}$ 224) and (062) planes of VS_4 . HAADF-STEM image and corresponding elemental mapping images of the VS_4 nanowire clusters (Fig. 1e) indicate the even distribution of V and S elements.

Nitrogen sorption isotherms of the VS_4 nanowire clusters (Figure S2) present typical H3 (type-IV) hysteresis, pointing the presence of slit-shaped mesopores [24]. The specific surface area is $46.25 \text{ m}^2 \text{ g}^{-1}$. As inset of Figure S2, Barrett-Joyner-Halenda pore size distribution curves indicate that the pore size distribution is basically between 0 and 50 nm with a mean pore size of $\sim 25.81 \text{ nm}$. The special structure of VS_4 can effectively raise the electrical conductance between each nanowire and promote the transport of electrons and Al^{3+} in electrochemical process, hence beneficial to rate capability and the exploitation ratio of active material.

Cyclic voltammetry (CV) was tested in 0.1–1.8 V versus $Al/AlCl_4$ at

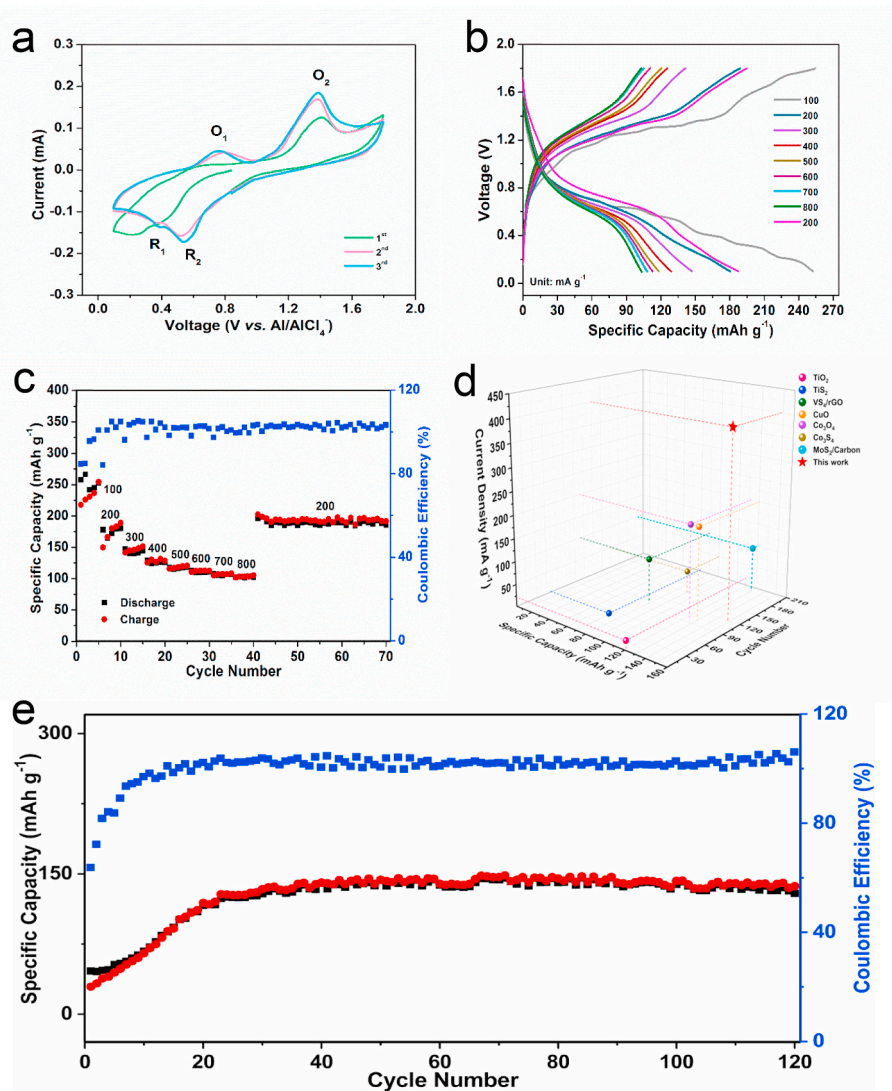


Fig. 2. Electrochemical performances of the VS₄ nanowire clusters for AlBs. (a) CV curves for the first three cycles. (b) The charge/discharge curves. (c) Rate performances at various current densities. (d) Comparison of cycling performance with other Al-storage materials. (e) Long-term cycling stability and coulombic efficiency.

0.1 mV s⁻¹ (Fig. 2a) to clarify the reaction mechanism of the VS₄ nanowire clusters. During the cathode reduction process, two peaks observed at 0.39 V versus Al/AlCl₄ (R₁) and 0.54 V (R₂) were the partial reduction of S₂²⁻ to S²⁻ and the partial oxidation of V⁴⁺ to V⁵⁺. While the corresponding oxidation peaks located at 0.75 V (O₁) and 1.38 V (O₂) were most V⁵⁺ and S²⁻ changes back to V⁴⁺ and S₂²⁻. The 2nd and 3rd curves almost overlap, displaying a remarkable cycling stability and excellent reversibility of the as-obtained VS₄ nanowire clusters electrode.

Figure S3 shows the charge/discharge curves of the VS₄ nanowire clusters at 400 mA g⁻¹ for various cycles. First cycle reveals discharge/charge capacities of 46.26/29.51 mAh g⁻¹, demonstrating major discharge plateaus at 0.39 V, and at approximately 1.38 and 1.56 V are charge plateaus, respectively. The discharge capacities of the 20th, 40th, 60th, 80th, 100th, and 120th cycles are calculated to be 116.48, 140.11, 142.99, 140.66, 138.89 and 129.24 mAh g⁻¹, respectively. Meanwhile, the plateaus of discharge occur near 0.67 and 0.35 V and the plateaus at 1.35 and 1.65 V is charge plateaus.

Charge-discharge cycles from 100 to 800 mA g⁻¹ were investigated to assess the rate performance of the VS₄ nanowire clusters (Fig. 2b). In Fig. 2c, a reduction in the specific capacity values is observed when the current density is increased. The discharge capacity maintained 252.51 mAh g⁻¹ after 5 cycles at 100 mA g⁻¹ and subsequently to 180.40, 147.04,

129.06, 118.32, 112.81, 108.02, and 103.32 mAh g⁻¹ after every 5 charge-discharge cycles corresponding to 200, 300, 400, 500, 600, 700, and 800 mA g⁻¹. The high rate performance of the VS₄ nanowire clusters electrode was affirmed as the electrode material successfully recovered a discharge capacity of 189.71 mAh g⁻¹ when current density was taken back to 200 mA g⁻¹. Besides, the VS₄ nanowire clusters achieved good cycling stability. These results could be ascribed to the channels-rich nanostructure towards which allows the effective passage and diffusion of electrolyte ions. To prove the superiority of the VS₄ nanowire clusters, we have synthesized VS₄ nanospheres and tested their electrochemical performance (Figure S4 and Figure S5).

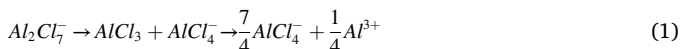
We compared the cycling property of related transition metal compound cathodes to illustrate the significance and importance of this work (Fig. 2d and Table S1) [18,25–30]. Fig. 2e shows cycling performance of the VS₄ nanowire clusters electrode at 400 mA g⁻¹ for 120 cycles. After a capacity augment in the initial cycles, after 120 cycles a reversible capacity of 129.24 mAh g⁻¹ can be remained and steady coulombic efficiency closed to 100%, attesting a superior long-term operation durability.

The capacity performance and coulombic efficiency of the battery at 800 mA g⁻¹ for 250 cycles as Figure S6 shown. The discharge specific capacity can still be remain 98.66 mAh g⁻¹, while a coulombic efficiency

of about 100% was maintained. As shown in Figure S7, the VS₄ nanowire clusters electrode has almost no morphological structure cracking, no phase change after undergoing long cycling. In general, this battery system has remarkable capacity performance and cycling stability. Such outstanding cycling performance of the VS₄ nanowire clusters electrode is largely due to the channels-rich nanowire clusters which can effectively reduce the pulverization of the structure during the storage process as well as facilitate the diffusion of the large-sized Al_xCl_y⁻ [16]. In the first 20 cycles, the capacity keeps rising in the course of the activation process and can be attributed to the incomplete reaction of the material [31,32].

Working mechanism schematic of the reversible Al/V_S₄ nanowire clusters battery is shown in Fig. 3a. As shown in Equation (1), Al₂Cl₇⁻ dissociation reaction resulting in Al³⁺ and AlCl₄⁻ reappear in the cathode. The generated Al³⁺ takes part in the insertion process in the VS₄ nanowire clusters as Equation (2). As Equation (3) shown, on the anode materials, aluminum resulting Al³⁺ combines with AlCl₄⁻ to form Al₂Cl₇⁻ and liberates three electrons [33]. Charging the battery reverses this process. In other metal sulfides, similar Al³⁺ insertion reaction was also found, such as Mo₆S₈ [34], MoS₂ [35] and TiS₂ [36], which other than the notion that ordinary metal sulfides commonly result in conversion reactions.

Cathode:



Anode:



To explore the storage behavior of aluminum, kinetic analyses were applied. Fig. 3b shows CV plots at different scan rates. Clearly, it has two pairs of redox peaks. The reduction peaks shift to the negative direction, the oxidation peaks move to the positive direction, with the scanning rate increases, revealing the existing electrochemical polarization.

The battery shows more diffusion-controlled battery characteristics. Equation (4) is used to clarify the relationship between scan rate (ν) and peak current (i) [37].

$$i = a\nu^b \quad (4)$$

And $b = 1$ represents capacitive-dominated charge storage, $b = 0.5$ discloses a semi-infinite linear diffusion-controlled charge storage [37]. The $\log(i)$ versus $\log(\nu)$ plots from 0.2 to 1.0 mV s⁻¹ for oxidation and reduction peaks as shown in Fig. 3c. After linear fitting, for the first pair oxidation and reduction peaks the b values are 0.75 and 0.81, while the b values are 0.92 and 0.87 for the second pair oxidation and reduction peaks, reflecting the fast reaction kinetics behavior.

To have a further insight into the electrochemical behavior, ex-situ EIS (electrochemical impedance spectra) studies were collected at full charge state during the long cycles at 400 mA g⁻¹. The lower right corner of Figure S8 is the close-up of the high-frequency region. As charge transfer resistance (R_{ct}) becomes much smaller after the 15th cycle and reduces further in the following cycles, indicating that the redox reaction activity increased. In the low frequency region, the slope gets higher and higher, and the diffusion coefficient increases. This indicates that the electrochemical reactivity is higher and higher as the cycle progresses. This is consistent with the long cycles.

Power density and energy density are recognized as the two major performance metrics for energy storage systems. The energy and power density of the VS₄ nanowire clusters were plotted and compared with other similar materials in Fig. 3d [18,25–30]. It is obvious that VS₄ nanowire clusters electrode presents the largest power density and energy density in comparison with other systems. The VS₄ nanowire clusters can bestow a high stable energy density of about 200 Wh kg⁻¹.

Fig. 4a-f shows the compositional characterizations of VS₄ electrodes during the different electrochemical processes. Fig. 4a displays the original VS₄ electrodes and the (110) plane is presented in Fig. 4d. After the initial discharge process in Fig. 4b, the (002) plane is found and the interlayer space increased, as presented in Fig. 4e. When charged to 1.8 V, as demonstrated in Fig. 4c and f, the interlayer space decreased in response, suggesting the crystallographic recovery of VS₄. Fast Fourier

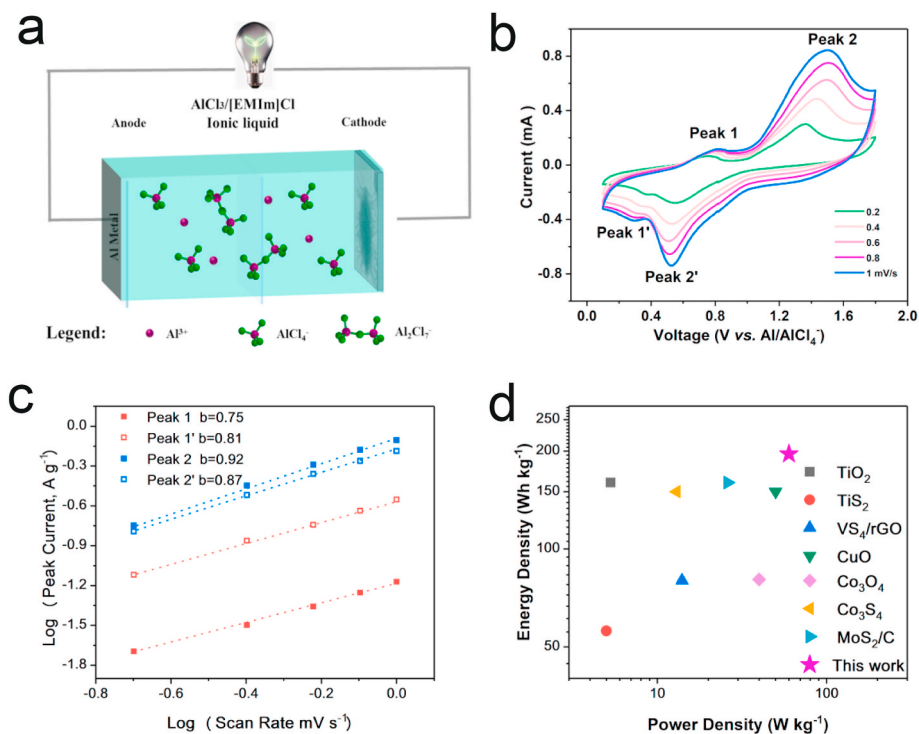


Fig. 3. (a) Working mechanism schematic of the rechargeable Al/V_S₄ nanowire clusters battery. (b) CV curves at different scan rates. (c) The normalized peak current vs. scan rate plots to determine the b -value for both oxidation and reduction peaks. (d) Ragone plot.

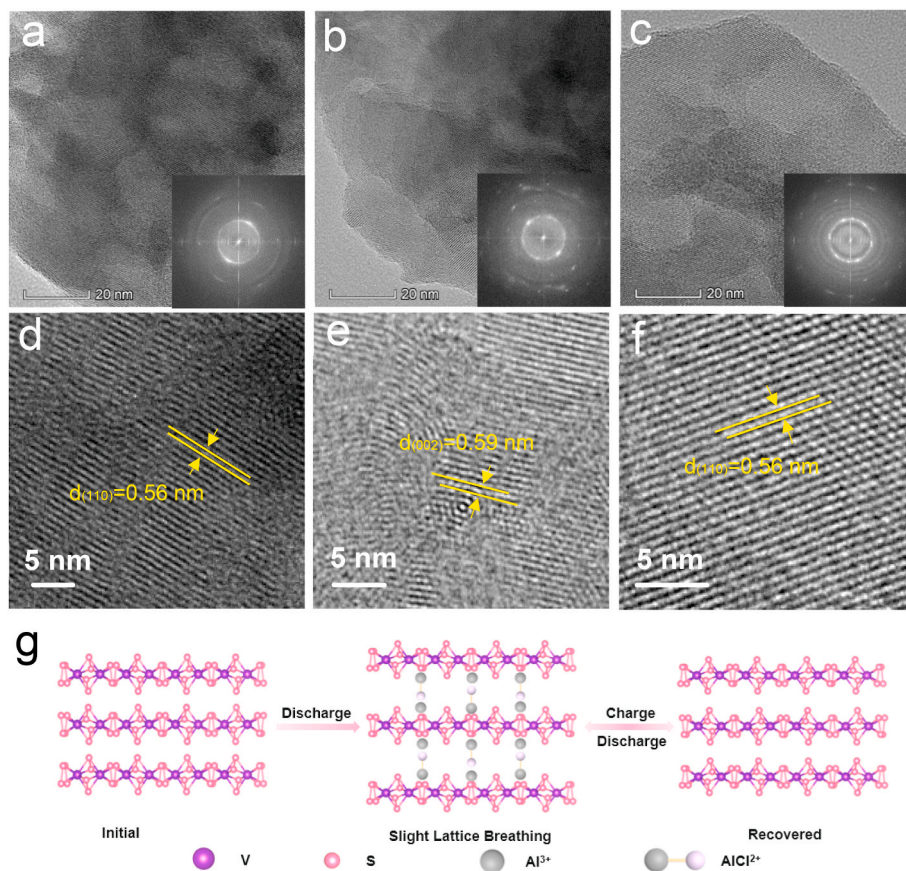


Fig. 4. (a-c) TEM images of original VS₄, discharged state, charged state in the initial cycle. Inside are corresponding FFT images. (d-f) HRTEM images corresponding to (a-c). (g) Schematic illustration of Al³⁺ intercalation/de-intercalation behavior into/from VS₄ at different processes.

Transform (FFT) patterns confirm the polycrystalline nature of the VS₄ electrodes at different charging states. According to the above results, the reaction mechanism of VS₄ is determined. The processes of intercalation and deintercalation on the VS₄ nanowire clusters surface are shown in Fig. 4g, further supporting the reversible intercalation and deintercalation. The channels-rich structure can shorten ion diffusion distance, enhance the electrolyte contact area, improve charge transfer and facilitate access of electrolyte ions.

To explore aluminum-storage mechanism and the valence changes of the VS₄ nanowire clusters electrode at different processes, Fig. 5a-d shows XPS measurements of VS₄ at V 2p, S 2p, Al 2p and Cl 2p regions obtained at different stages. The high-resolution V 2p XPS spectrum of pristine VS₄ nanowire clusters (Fig. 5a) displays two main peaks are connected with V 2p_{1/2} and V 2p_{3/2} orbital. After discharging to 0.1 V, the energy bands intensities of V 2p_{1/2} band at 524.48 eV and V 2p_{3/2} band at 517.02 eV of V⁵⁺ obviously increased which demonstrate the partial oxidation of V⁴⁺ to V⁵⁺. When charged to 1.8 V, the V 2p XPS spectrum still could be deconvoluted into four peaks.

High-resolution S 2p XPS spectrum of pristine VS₄ nanowire clusters appears two peaks at 164.05 and 162.89 eV in Fig. 5b, corresponding to the S 2p_{1/2} and S 2p_{3/2} bands for S₂²⁻. After discharge, peaks of S₂²⁻ weaken and two new peaks of S²⁻ appeared at 163.84 eV (S 2p_{1/2} band) and 162.76 eV (S 2p_{3/2} band), meaning that a part of S₂²⁻ is reduced to S²⁻ when Al³⁺ intercalates into the VS₄. After recharged to 1.8 V, four peaks are obtained from fitting the S 2p high-resolution spectrum. Two peaks at 164.04 and 162.62 eV belong to S₂²⁻, other peaks at 162.89 and 164.02 eV are ascribed to S₂²⁻.

There are some Al³⁺ remaining in the VS₄ lattices during the electrochemical reactions (Fig. 5c). After the first discharge step the intensity of Al 2p band is higher than after charge step, confirming the reversible intercalation/de-intercalation of Al³⁺ into/from VS₄.

Compared with pristine VS₄ nanowire clusters, the Al 2p and Cl 2p signals in VS₄ simultaneously appear when discharging to 0.1 V, and the peak intensities concurrently decrease again on charging back to 1.8 V (Fig. 5c and d), revealing that Al and Cl atoms are together inserted into the structural interlayer.

The *ex-situ* XRD patterns at various states of the VS₄ nanowire clusters (from pristine, after discharging to 0.1 V and charging to 1.8 V) were measured, as shown in Fig. 5e. The diffraction peak located at about 17.8° was attributed to polytetrafluoroethylene (PTFE) (Figure S9). A small structural change of VS₄ occurs during Al³⁺ insertion/extraction processes. The (114) peak there is a slight shift during discharge. However, the intensities of these peaks changed (Fig. 5f). During the discharge process, no obvious shifts of the characteristic peaks are observed, which unveils the existence of single-phase solid solution reaction of VS₄ for Al³⁺ storage [32]. In the subsequent charge process, the slight shift peak recovered to its original state.

To understand the chloroaluminate anions intercalation/deintercalation of VS₄ nanowire clusters electrode, *in-situ* Raman spectroscopy was investigated (Fig. 5g). V-S bonds at 191.09 and 222.24 cm⁻¹ are attributed to the stretching modes while the bond at 272.15 cm⁻¹ corresponds to the bending mode (Figure S10) [38]. The peaks at 301.72 and 559.45 cm⁻¹ are S-S bond stretching/twisting [39,40]. The peak located at 347.67 cm⁻¹ is a breathing mode of the V₂S₄ cages [41]. At different processes, these peak positions changed obviously. At the first discharge step, the Raman peaks became weaker, suggesting that Al³⁺ was inserted into VS₄. Then, the peak intensities gradually recovered again during the first charge step, because of the incomplete extraction of Al³⁺ [41]. The peaks located at 415.45, 573.63 and 746.21 cm⁻¹ throughout the whole discharging and charging process are due to the base of sapphire (Figure S11). At the second discharge step, the Raman peaks become weaker again. These results indicate the good reversibility

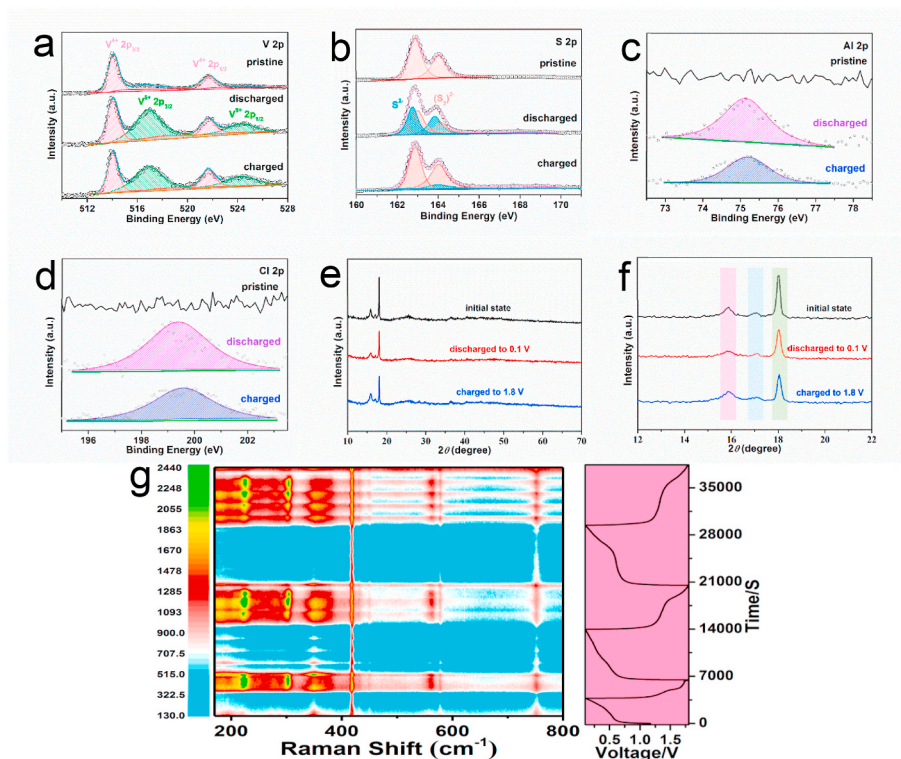


Fig. 5. (a-d) XPS spectra at V 2p (a), S 2p (b), Al 2p (c) and Cl 2p (d) regions of the VS₄ nanowire clusters at different states. (e) *Ex-situ* XRD patterns at various states of VS₄ cathode. (f) Enlargement of selected regions. (g) *In-situ* Raman spectra of VS₄ cathode and its corresponding curves of charge-discharge at 100 mA g⁻¹ for the first to third cycles.

of Al³⁺ insertion/extraction.

HAADF-STEM with energy-dispersive X-ray spectroscopy (EDS) was obtained to further explore the Al³⁺ intercalation in the VS₄ nanowire clusters. As shown in Figure S12a, in discharged state, V, S, Al and Cl elements have the uniform distribution through the VS₄ particle region, which verifies the insertion of Al³⁺ and Cl⁻ into the VS₄. In Figure S12b, in the charged state, Al and Cl signals were still spotted but with much faintish intensities through the VS₄ region juxtaposed with that of the discharged state. The outcome means that in the charging process the Al³⁺ and Cl⁻ in the VS₄ electrode cannot be extracted entirely, which is in compliance with the XPS results.

3. Conclusion

In conclusion, the channels-rich VS₄ nanowire clusters are prepared via an amine-ion assisted method. The VS₄ nanowire clusters electrode exhibits high Al storage capacity (252.51 mAh g⁻¹) and superior rate performance (103.32 mAh g⁻¹ at 800 mA g⁻¹). As compared to the reported Al³⁺ intercalation materials, the fast kinetics enable the excellent rate capability and better specific capacity. From above results, VS₄ could maintain its structural stability when Al³⁺ insert/extract from the layered spacing and this makes it a potential cathode material for AIBs. All these results shed new light on discovering novel metal chalcogenides as electrodes and this material is anticipated to give a profound influence on the development of rechargeable AIBs.

4. Experimental section

4.1. Fabrication of the VS₄ nanowire clusters

The synthesis of VS₄ was modified through a conventional method [41]. First, in a typical procedure, 500 mg of Pluronic® F127 and 350 mg of ammonium metavanadate were introduced into 30 mL deionized water. Then white suspension liquid was heated at 60 °C to form a

yellow solution A. Next, 1000 mg of thioacetamide (TAA) was dissolved in 30 mL of ethylene glycol noted as solution B. Admixed solution A with B by stirring at 60 °C. The resultant mixture was poured into a 100 mL autoclave and heated at 160 °C for 10 h. Finally, dark brown precipitates were obtained after centrifuging and freeze drying. As a comparison, the VS₄ nanospheres were synthesized via the same amine ions-assisted method, but without adding Pluronic® F127.

4.2. Preparation of ionic liquid electrolyte and sample for the XPS measurement

Anhydrous aluminum chloride (Sigma-Aldrich, AlCl₃, 99.999%) was slowly added in 1-ethyl-3-methylimidazolium chloride (Aladdin, [EMIm]Cl, 98%) with a molar ratio of 1.3:1 in a glove box under rigid stirring. A pale yellow transparent liquid was obtained.

First, the VS₄ cathode were discharged to 0.1 V (or charged to 1.8 V) at 50 mA g⁻¹. After the end of discharging (charging) process, be careful not to short-circuit, the cells were disassembled promptly. Then, the electrodes were washed with acetonitrile and then dried naturally in a glove box.

4.3. Material characterization

X-ray diffraction (XRD) and *ex-situ* XRD were obtained with Bruker D2 Phaser use Cu K α radiation source. Raman and *in-situ* Raman spectra were accomplished by a HORIBA LabRAM HR Evolution microRaman spectroscopy system with an excitation laser wavelength of $\lambda = 532$ nm. Scanning electron microscopy (SEM) images were recorded using a JEOL-7100F microscope. Transmission electron microscopy (TEM), high resolution TEM (HRTEM) and scanning TEM-high-angle annular dark-field (HAADF) images were obtained with a Talos F200S. X-ray photoelectron spectroscopy (XPS) measurements were performed by ESCALAB 250Xi. Brunauer-Emmett-Teller (BET) surface area was tested through Tristar II 3020 instrument.

4.4. Electrochemical tests

Electrochemical measurements were performed by assembling 2016 coin-type cells using aluminum foil as the anode, Whatman glass microfiber filters (GF/A) as the separator, and molybdenum foil as the current collector. The working electrode was prepared from 60% active material, 30% acetylene black and 10% polytetrafluoroethylene (PTFE). The slurry was evenly grinded and then dried at 60 °C overnight. The electrode was cut into 0.6 × 0.6 cm². The mass loading of active material on each electrode was about 1.5 mg. Cyclic voltammetry (CV) tests were performed by Autolab PGSTAT302 N. Galvanostatic discharge/charge tests were studied in 0.1–1.8 V versus AlCl₄/Al on a NEWARE battery testing system. Electrochemical impedance spectra (EIS) measurements were recorded at a stable open-circuit potential using amplitude of 10.0 mV in the frequency range of 100 kHz–0.01 Hz at different cycles.

CRediT authorship contribution statement

Lingli Xing: Conceptualization, Methodology, Validation, Investigation, Data curation, Writing - original draft, Writing - review & editing. **Kwadwo Asare Owusu:** Writing - review & editing, Formal analysis. **Xinyu Liu:** Validation, Formal analysis. **Jiashen Meng:** Conceptualization, Formal analysis. **Kun Wang:** Conceptualization, Supervision. **Qinyou An:** Conceptualization, Supervision. **Liqiang Mai:** Conceptualization, Supervision.

Declaration of competing interest

The authors declare that they have no known competing financial interests or personal relationships that could have appeared to influence the work reported in this paper.

Acknowledgements

This work was supported by the National Natural Science Foundation of China (51832004, 51521001), the National Key Research and Development Program of China (2016YFA0202603), the Program of Introducing Talents of Discipline to Universities (B17034), Foshan Xianhu Laboratory of the Advanced Energy Science and Technology Guangdong Laboratory (XHT2020-003).

Appendix A. Supplementary data

Supplementary data to this article can be found online at <https://doi.org/10.1016/j.nanoen.2020.105384>.

References

- [1] M. Armand, J.M. Tarascon, *Nature* 451 (2008) 652–657.
- [2] J. Wu, Y. Cao, H. Zhao, J. Mao, Z. Guo, *Carbon Energy* 1 (2019) 57–76.
- [3] S. Zhu, C. Chen, P. He, S. Tan, F. Xiong, Z. Liu, Z. Peng, Q. An, L. Mai, *Nano Res* 12 (2019) 1371–1374.
- [4] R. Gummow, G. Vamvounis, M. Kannan, Y. He, *Adv. Mater.* 30 (2018), 1801702.
- [5] D. Aurbach, Z. Lu, A. Schechter, Y. Gofer, H. Gizbar, R. Turgeman, Y. Cohen, M. Moshkovich, E. Levi, *Nature* 407 (2000) 724–727.
- [6] H. Hong, J. Liu, H. Huang, C. Etogo, X. Yang, B. Guan, L. Zhang, *J. Am. Chem. Soc.* 141 (2019) 14764–14771.
- [7] H. Wang, X. Bi, Y. Bai, C. Wu, S. Gu, S. Chen, F. Wu, K. Amine, J. Lu, *Adv. Energy Mater* 7 (2017), 1602720.
- [8] F. Wu, H. Yang, Y. Bai, C. Wu, *Adv. Mater.* 31 (2019), 1806510.
- [9] L. Wu, R. Sun, F. Xiong, C. Pei, K. Han, C. Peng, Y. Fan, W. Yang, Q. An, L. Mai, *Phys. Chem. Chem. Phys.* 20 (2018) 22563–22568.
- [10] A. Jadhav, J. Xu, R. Messinger, *ACS Energy Lett* 5 (2020) 2842–2848.
- [11] M. Lin, M. Gong, B. Lu, Y. Wu, D. Wang, M. Guan, M. Angell, C. Chen, J. Yang, B. Hwang, H. Dai, *Nature* 520 (2015) 324–328.
- [12] S. Das, *Angew. Chem. Int. Ed.* 57 (2018) 16606–16617.
- [13] J. Liu, Z. Li, X. Huo, J. Li, *J. Power Sources* 422 (2019) 49–56.
- [14] X. Zhang, G. Zhang, S. Wang, S. Li, S. Jiao, *J. Mater. Chem.* 6 (2018) 3084–3090.
- [15] Y. Hu, B. Luo, D. Ye, X. Zhu, M. Lyu, L. Wang, *Adv. Mater.* 29 (2017), 1606132.
- [16] T. Cai, L. Zhao, H. Hu, T. Li, X. Li, S. Guo, Y. Li, Q. Xue, W. Xing, Z. Yan, L. Wang, *Energy Environ. Sci.* 11 (2018) 2341–2347.

- [17] H. Li, H. Yang, Z. Sun, Y. Shi, H. Cheng, F. Li, *Nano Energy* 56 (2019) 100–108.
- [18] W. Yang, H. Lu, Y. Cao, B. Xu, Y. Deng, W. Cai, *ACS Sustain. Chem. Eng.* 7 (2019) 4861–4867.
- [19] W. Xing, D. Du, T. Cai, X. Li, J. Zhou, Y. Chai, Q. Xue, Z. Yan, *J. Power Sources* 401 (2018) 6–12.
- [20] X. Yu, L. Yu, L. Shen, X. Song, H. Chen, X. Lou, *Adv. Funct. Mater.* 24 (2014) 7440–7446.
- [21] S. Zhu, Q. Li, Q. Wei, R. Sun, X. Liu, Q. An, L. Mai, *ACS Appl. Mater. Interfaces* 9 (2017) 311–316.
- [22] Q. Li, L. Li, P. Wu, N. Xu, L. Wang, M. Li, A. Dai, K. Amine, L. Mai, J. Lu, *Adv. Energy Mater* 9 (2019), 1901153.
- [23] R. Wang, Y. Han, Z. Wang, J. Jiang, Y. Tong, X. Lu, *Adv. Funct. Mater.* 28 (2018), 1802157.
- [24] J. Li, J. Li, D. Yan, S. Hou, X. Xu, T. Lu, Y. Yao, W. Mai, L. Pan, *J. Mater. Chem.* 6 (2018) 6595–6605.
- [25] T. Koketsu, J. Ma, B. Morgan, M. Body, C. Legein, W. Dachraoui, M. Giannini, A. Demortiere, M. Salanne, F. Dardoize, H. Groult, O. Borkiewicz, K. Chapman, P. Strasser, D. Dambournet, *Nat. Mater.* 16 (2017) 1142–1148.
- [26] L. Geng, J. Scheifers, C. Fu, J. Zhang, B. Fokwa, J. Guo, *ACS Appl. Mater. Interfaces* 9 (2017) 21251–21257.
- [27] X. Zhang, S. Wang, J. Tu, G. Zhang, S. Li, D. Tian, S. Jiao, *ChemSusChem* 11 (2018) 709–715.
- [28] X. Zhang, G. Zhang, S. Wang, S. Lia, S. Jiao, *J. Mater. Chem.* 6 (2018) 3084–3090.
- [29] J. Liu, Z. Li, X. Huo, J. Li, *J. Power Sources* 422 (2019) 49–56.
- [30] H. Li, H. Yang, Z. Sun, Y. Shi, H. Cheng, F. Li, *Nano Energy* 56 (2019) 100–108.
- [31] Y. Xu, X. Deng, Q. Li, G. Zhang, F. Xiong, S. Tan, Q. Wei, J. Lu, J. Li, Q. An, L. Mai, *Inside Chem.* 5 (2019) 1194–1209.
- [32] X. Xu, M. Duan, Y. Yue, Q. Li, X. Zhang, L. Wu, P. Wu, B. Song, L. Mai, *ACS Energy Lett* 4 (2019) 1328–1335.
- [33] S. Wang, S. Jiao, J. Wang, H. Chen, D. Tian, H. Lei, D. Fang, *ACS Nano* 11 (2016) 469–477.
- [34] L. Geng, G. Lv, X. Xing, J. Guo, *Chem. Mater.* 27 (2015) 4926–4929.
- [35] Z. Li, B. Niu, J. Liu, J. Li, F. Kang, *ACS Appl. Mater. Interfaces* 10 (2018) 9451–9459.
- [36] L. Geng, J. Scheifers, C. Fu, J. Zhang, B. Fokwa, J. Guo, *ACS Appl. Mater. Interfaces* 9 (2017) 21251–21257.
- [37] Z. Le, F. Liu, P. Nie, X. Li, X. Liu, Z. Bian, G. Chen, H. Wu, Y. Lu, *ACS Nano* 11 (2017) 2952–2960.
- [38] H. Qin, Z. Yang, L. Chen, X. Chen, L. Wang, *J. Mater. Chem.* 6 (2018) 23757–23765.
- [39] Z. Li, B. Vinayan, P. Jankowski, C. Njel, A. Roy, T. Vegge, J. Maibach, J. Lastra, M. Fichtner, Z. Karger, *Angew. Chem. Int. Ed.* 59 (2020) 11483–11490.
- [40] M. Kozlova, Y. Mironov, E. Grayfer, A. Smolentsev, V. Zaikovskii, N. Nebogatikova, T. Podlipskaya, V. Fedorov, *Chem. Eur J.* 21 (2015) 4639–4645.
- [41] Y. Wang, Z. Liu, C. Wang, X. Yi, R. Chen, L. Ma, Y. Hu, G. Zhu, T. Chen, Z. Tie, J. Ma, J. Liu, Z. Jin, *Adv. Mater.* 30 (2018), 1802563.



Lingli Xing received her M.S. degree from Xinyang Normal University in 2018. She is currently working toward the Ph.D. degree in Materials Science and Engineering from Wuhan University of Technology (WUT). Her current research focuses on synthesis and characterization of advanced materials for aluminum-ion batteries.



Kwadwo Asare Owusu received his BSc degree in Materials Engineering from Kwame Nkrumah University of Science and Technology, Ghana (2012) and earned M.S. (2016) and Ph.D. (2020) degrees from WUT under the supervision of Prof. Liqiang Mai. His current research is on new nanomaterials for high energy supercapacitors and post-lithium ion batteries.



Xinyu Liu is an undergraduate student and in Department of Materials Science and Engineering from WUT since 2018. He has joined WUT Nano Key Laboratory for two years. His current research focuses on the electrochemical energy storage materials and devices.



Qinyou An is Associate Professor of Materials Science and Engineering at WUT. He received his Ph.D. degree from WUT in 2014. He carried out his postdoctoral research in the laboratory of Prof. Yan Yao at the University of Houston in 2014–2015. Currently, his research interest includes energy storage materials and devices.



Jiashen Meng received his B.S. degree from WUT in 2015 and he received his Ph.D. in 2020 in Materials Science at WUT. From 2018 to 2019, he was a visiting Ph.D. student in Prof. Donald Sadoway's group at Massachusetts Institute of Technology. His current research focuses on developing new nanomaterials and chemistry for energy conversion and storage devices.



Liqiang Mai is the Chair professor of Materials Science and Engineering at WUT, Dean of School of Materials Science and Engineering at WUT, Fellow of the Royal Society of Chemistry. He received his Ph.D. from WUT in 2004 and carried out his postdoctoral research at Georgia Institute of Technology in 2006–2007. He worked as an advanced research scholar at Harvard University and University of California, Berkeley. His current research interests focus on new nanomaterials for electrochemical energy storage and micro/nano energy devices.



Kun Wang has BS and MS degrees in Materials Science and Engineering from the WUT, China and a Ph.D. in Materials Engineering from the Monash University, Australia. Following a postdoctoral fellowship at Monash University in Australia, she joined WUT, China, where she is currently Associate Professor in the State Key Laboratory of Silicate Materials for Architectures. From then, she teaches and conducts research in the synthesis and processing of advanced materials, focusing on ceramics and nanomaterials.